Journal of Nuclear Medicine, published on March 13, 2020 as doi:10.2967/jnumed.119.239731

Design and development of ^{99m}Tc-labeled FAPI-tracers for SPECT-imaging and ^{188}Re therapy.

Thomas Lindner[1], Annette Altmann[1,2], Susanne Krämer[1], Christian Kleist[1], Anastasia Loktev[1,2], Clemens Kratochwil[1], Frederik Giesel[1], Walter Mier[1], Frederik Marme[5], Jürgen Debus[3,4], Uwe Haberkorn [1,2,6, §]

(1) Department of Nuclear Medicine, University Hospital Heidelberg, Heidelberg Germany.
(2) Clinical Cooperation Unit Nuclear Medicine, German Cancer Research Center (DKFZ), Heidelberg, Germany.
(3) Dept. of Radiation Oncology, University Hospital Heidelberg, Heidelberg, Germany
(4) Clinical Cooperation Unit Radiation Oncology, German Cancer Research Center (DKFZ), Heidelberg, Germany
(5) Translational Gynecologic Oncology, University Hospital Mannheim, Germany
(6) Translational Lung Research Center Heidelberg (TLRC), German Center for Lung Research (DZL), Heidelberg, Germany

[§]Corresponding author:

Uwe Haberkorn

Department of Nuclear Medicine

University Hospital Heidelberg

Im Neuenheimer Feld 400

69120 Heidelberg

Tel: +49-6221-56-7732

Fax: +49-6221-56-5473

Email: uwe.haberkorn@med.uni-heidelberg.de

^{99m}Tc-labeled FAPI tracers

First author:

Thomas Lindner

Department of Nuclear Medicine

University Hospital Heidelberg

Im Neuenheimer Feld 400

69120 Heidelberg

Tel: +49-6221-56-7726

Email: Thomas.Lindner@med.uni-heidelberg.de

Conflicts of interest: Patent application (EP 18155420.5) for quinoline based FAP targeting agents for imaging and therapy in nuclear medicine (UH, AL, TL, CK, FG and WM).

Keywords: Fibroblast activating protein, SPECT, theranostics, small molecule inhibitor

Word count: 5057

ABSTRACT

The majority of epithelial tumors recruits fibroblasts and other non-malignant cells and activates them into cancer-associated fibroblasts. This often leads to overexpression of the membrane serine protease fibroblast-activating protein (FAP). It has already been shown that DOTA-bearing FAP inhibitors (FAPIs) generate high contrast images with PET/CT scans. Since SPECT is a lower cost and more widely available alternative to PET, ^{99m}Tc-labeled FAPIs represent attractive tracers for imaging applicable in a larger number of patients. Furthermore, the chemically homologous nuclide ^{188}Re is available from generators, which allows FAP-targeted endoradiotherapy.

Methods: For the preparation of ^{99m}Tc tricarbonyl complexes, a chelator was selected whose carboxylic acids can easily be converted into various derivatives in the finished product. This enabled a platform strategy based on the original tracer. The obtained ^{99m}Tc complexes were investigated *in vitro* by binding and competition experiments on FAP-transfected HT-1080 (HT-1080-FAP) and/or on mouse FAP expressing (HEK-muFAP) and CD26-expressing (HEKCD26) HEK cells and characterized by planar scintigraphy and organ distribution studies in tumor-bearing mice. Furthermore, a first-in-man application was done in two patients with ovarian and pancreatic cancer, respectively.

Results: ^{99m}Tc-FAPI-19 showed specific binding to recombinant FAP-expressing cells with high affinity. Unfortunately, liver accumulation, biliary excretion and no tumor uptake were observed in the planar scintigraphy of a HT-1080-FAP xenotranplanted mouse. To improve the pharmacokinetic properties hydrophilic amino acids were attached to the chelator moiety of the compound. The resulting ^{99m}Tc-labeled FAPI tracers revealed excellent binding properties (up to 45 % binding; above 95 % internalization), high affinity (IC_{50} = 6.4 nM to 12.7 nM), and significant tumor uptake (up to 5.4 %ID/g) in biodistribution studies. The lead candidate ^{99m}Tc-FAPI-34 was applied for diagnostic scintigraphy and SPECT of patients with metastasized ovarian and pancreatic cancer for follow-up to therapy with ^{90}Y-FAPI-46. ^{99m}Tc-FAPI-34 accumulated in the tumor lesions also shown in PET/CT imaging using ^{68}Ga-FAPI-46.

Conclusion: ^{99m}Tc-FAPI-34 represents a powerful tracer for diagnostic scintigraphy, especially in cases where PET imaging is not available. Additionally, the chelator used in this compound allows labeling with the therapeutic nuclide ^{188}Re which is planned for the near future.

INTRODUCTION

While in the classical approach mainly tumor cells were the sole target for cancer therapy, tumor microenvironment and tumor stroma came increasingly into focus to enable novel forms of treatment. Cancer-associated fibroblasts (CAFs) are an important component in a large number of neoplasias as they actively contribute to tissue remodeling, resistance development and immune evasion (*1*). CAFs can be formed from different progenitors resulting in variations of their proteome. However, many CAFs are characterized by an overexpression of the fibroblast activating protein (FAP) (*2,3*). This protein is a membrane-bound serine protease with both dipeptidyl peptidase and endopeptidase activity that hydrolyzes denatured collagen type 1, among other substrates. Since FAP is almost absent in healthy tissue, inhibitors of FAP (FAPIs) can be used in nuclear medicine for PET-imaging and possibly also for endoradiotherapy of a variety of cancers with desmoplastic reaction such as pancreatic, breast and colon carcinomas (*4-10*).

Employing ^{68}Ga-labeled FAPIs for preclinical and clinical PET/CT imaging, we observed a very high rate of internalization of the tracer but also a considerable efflux. This resulted in relatively short intratumoral half-lives (*5,11*). For a therapeutic application of this family of compounds the physical half-life of the radionuclide used for labeling has to be adjusted to the biological half-life in the tumor. Therefore, ^{177}Lu or ^{225}Ac which have been applied successfully for the targeted treatment of neuroendocrine tumors and prostate cancer are not useful in this context. In contrast, short lived isotopes such as the alpha emitter ^{213}Bi or the beta emitter ^{188}Re may deliver higher doses to the tumor. However, whereas ^{213}Bi can be used for the molecules developed so far, labeling of FAPIs with ^{188}Re requires a different chelator coupled to the binding moiety. Chelators binding ^{188}Re could be also used for labeling with ^{99m}Tc for scintigraphy and SPECT.

Therefore, the goal of this project was twofold: the development of a tracer for endoradiotherapy with ^{188}Re and for widespread scintigraphic diagnostics with ^{99m}Tc.

MATERIALS AND METHODS

Synthesis and Radiolabeling

A detailed description of the synthetic pathway and protocols can be found in the supporting information (Supplemental Fig. 1). Labeling was performed with 100-150 MBq Na[$^{99m}TcO_4$] in 1 mL 0.9 % saline which was added to a CRS kit for tricarbonyl complexes (PSI, Villingen, Switzerland). The mixture was heated to 95 °C for 20 min to provide the intermediate [$^{99m}Tc(H_2O)_3(CO)_3]^+$ complex. After cooling to room temperature 200 µL of the solution were added to a mixture of 5 µL of the individual precursor (1 mM in water), 30 µL phosphate buffer (0.4 M; pH 7.4) and 45 µL hydrochloric acid (1 M) resulting in a pH of 5-6. The reaction was heated to 95 °C for 20 min and completeness was checked by radio-HPLC. The ^{99m}Tc-labeled tracers (ca. 250-500 nmol/GBq with regard to precursor amount) were used directly for *in vitro* studies or processed by solid phase extraction, evaporation and formulation with 0.9 % saline prior to imaging or biodistribution experiments.

Cell Culture

Binding properties of ^{99m}Tc labeled FAPI derivatives were evaluated using HT-1080 cells stably transfected with the human FAP-gene (HT-1080-FAP) as well as mouse FAP gene (HEK-muFAP) and human CD26 (HEKCD26) transfected human embryonic kidney cells (obtained from Stefan Bauer, NCT Heidelberg (*12*)). The cells were cultivated in Dulbecco's modified Eagle's medium (DMEM) containing 10 % fetal calf serum at 37 °C/5 % carbon dioxide.

Radioligand binding studies were performed as described previously (*4,5*). In brief, recombinant cells were seeded in 6-well plates and cultivated for 48 h to a final confluence of approx. 80-90 % (1.2 to $2x10^6$ cells/well). The medium was replaced by 1 mL fresh medium without fetal calf serum. The radiolabeled compound was added to the cell culture and incubated for different time intervals ranging from 10 min to 240 min. Competition experiments were performed by simultaneous exposure to unlabeled (10^{-5} M to 10^{-10} M) and radiolabeled compound for 60 min. In all experiments, the cells were

washed twice with 1 mL phosphate-buffered saline (PBS) pH 7.4 and subsequently lysed with 1.4 mL lysis buffer (0.3 M NaOH, 0.2 % SDS).

For internalization experiments the cells were incubated with the radiolabeled compound for 60 min and 240 min at 37 °C. Cellular uptake was terminated by removing medium from the cells and washing twice with 1 mL PBS. Subsequently, cells were incubated with 1 mL of glycine-HCl (1 M, pH 2.2) for 10 min at room temperature to harvest the surface bound peptides (glycine fraction). Thereafter, the cells were washed with 2 mL of ice-cold phosphate-buffered saline and lysed as described to determine the internalized (lysed) fraction. Radioactivity was determined in a Wizard Gamma Counter (Perkin Elmer), normalized to 1 x 10^6 cells and calculated as percentage of the applied dose (%AD). Each experiment was performed 3 times, and 3 repetitions per independent experiment were acquired.

Animal Studies

For in vivo experiments, 8 week old BALB/c nu/nu mice (Charles River) were subcutaneously inoculated into the right trunk with 5 × 10^6 HT-1080-FAP cells. When the size of the tumor reached approximately 1 cm^3, the radiolabeled compound was injected via the tail vein (2-5 MBq in 100 µL 0.9 % saline for small-animal imaging and 1 MBq in 100 µL 0.9 % saline for organ distribution). For organ distribution, the animals (n = 6 or n = 3 for each time point) were sacrificed at 1 h and 4 h or at different time points (30 min to 24 h) after tracer administration. The distributed radioactivity was measured in all dissected organs and in blood using a γ-counter (Cobra Autogamma, Packard). The values are expressed as percentage of injected dose per gram of tissue (%ID/g). Scintigraphic images were obtained using a γ camera (Gamma Imager, Biospace, France) with a recording time of 10 min per image. For the in vivo blockade experiments 30 nmol of unlabeled FAPI was added to the radiolabeled compound directly before injection.

All animal experiments were conducted in compliance with the German animal protection laws (permission number 35-91185.81/G-158/15).

Scintigraphy and SPECT/CT-Imaging

The patients gave written informed consent to receive FAPI-PET/CT, FAPI therapy and FAPI scintigraphy following the regulations of the German Pharmaceuticals Act §13(2b). All patients were referred to the experimental diagnostics by their caring oncologist, which were facing an unmet diagnostic challenge, which could not be solved sufficiently with standard diagnostic means. The data were analyzed retrospectively with approval of the local ethics committee (No. S016/2018).

The ^{99m}Tc-FAP-34 was applied via i.v. catheter as a bolus injection of 660 MBq via a sterile filter system (Filtropur S 0.2, Sarstedt, Nuembrecht, Germany). Whole body planar scintigraphy was performed at 10 minutes, 1, 4 and 20 h and a two bed position SPECT/CT at 4 h after tracer administration.

Scintigraphic images were performed using a low energy high resolution (LEHR) collimating system with an acquisition time of 1 min / 15 cm body height in a 1025 x 256 matrix. SPECT imaging acquisition was realized in a Infinia scanner system (GE Healthcare, Chalfont St Giles, Buckinghamshire, UK) using a 128 x 128 matrix, Zoom = 1, step by step scan by 30 sec and 120 images with 3 degrees angle cut in a 128 x 128 matrix. For FAPI-34 imaging a 4 slices low dose x-ray computed tomography (SPECT/CT) was performed for attenuation correction and general localization of FAPI-positive lesions.

PET/CT imaging was performed on a Biograph mCT Flow scanner (Siemens, Erlangen, Germany). Following non-contrast-enhanced low-dose CT (130keV, 30mAs, CareDose; reconstructed with a soft-tissue kernel to a slice thickness of 5mm), PET was acquired in 3-D mode (matrix 200×200) using FlowMotion (Siemens). The emission data were corrected for randoms, scatter and decay. Reconstruction was performed with an ordered subset expectation maximization (OSEM) algorithm with 2 iterations / 21 subsets and Gauss-filtered to a transaxial resolution of 5 mm at full-width at half-maximum (FWHM); Attenuation correction was performed using the non-enhanced low-dose CT data. The synthesis and labeling of FAPI-46 was done as described previously (*11*). The injected activity for the ^{68}Ga-FAPI-46 (*11*) exams was 260 MBq and the PET scans were started 1h post injection. 500ml saline

with 20mg Lasix was infused from 15 min before to 30 min after tracer application. The patients were asked to self-report any abnormalities 30 min after finishing the examination.

RESULTS

Synthesis of the Compounds

Detailed results of the individual synthetic steps can be found in the supporting information. An overview of FAPI-19 and corresponding FAPI derivatives is presented in Figure 1. Additionally, logP and plasma protein binding as well as the proteolytic stability were determined showing similar binding for all FAPI compounds (Supplemental Table 1) and, exemplarily, the high stability of ^{99m}Tc-FAPI-34 over 4 h (Supplemental Fig. 2).

FAPI-19 Shows High Accumulation in Tumor Cells but Unfavorable Pharmacokinetics

The first ^{99m}Tc labeled derivative FAPI-19 showed a binding of 35.8±1.0 % to 1 x10^6 HT-1080-FAP cells after 1 h which increased to 41.6±1.0 % after 4 h incubation (Fig. 2A) and a high internalization rate of above 95 % (Supplemental Table 2). Binding of ^{99m}Tc-FAPI-19 was suppressed entirely by addition of 10^{-7} M unlabeled FAPI-19 (Fig. 2B) demonstrating specificity and high affinity of this compound with an IC_{50}-value of 6.4 nM (Fig. 1). To ensure the ^{99m}Tc chelator does not affect specificity a binding experiment was conducted with two HEK cell lines transfected with either murine FAP (HEK-muFAP) or the closely related human membrane protein DPP4/CD26 (HEKCD26). Both, murine FAP and CD26 show a high homology to human FAP (muFAP: 90% identity and 94 % similarity on amino acid level; CD26: 52 % identity and 71 % similarity with high structural resemblance) (*13*). As expected from previous experiments performed with DOTA-modified FAPI derivatives(*4,5*) we measured significant binding to

murine FAP expressing cells (36.13±2.23 %) after 60 min, but almost no binding to CD26 expressing cells (0.2±0.02 %; Supplemental Table 3).

Due to the promising results *in vitro* ^{99m}Tc-labeld FAPI-19 was investigated as imaging agent in planar scintigraphy in a HT-1080-FAP xenotranplanted mouse. As shown in Figure 3A and Supplemental Figure 3A no tumor accumulation could be observed while the major portion of radioactivity was located in the liver. Besides a small fraction which is located in the bladder, the biliary elimination is observable by signals from the intestine after 30 min (Supplemental Fig. 3A). The circulating fraction is slightly detecteable after 120 min and has vanished at 4 h, while a significant part of the activity is still located in the liver at 120 min and is recognisable therein 4 h after injection.

Additional Hydrophilic Amino Acids Suppress Liver Accumulation and Hepatobiliary Excretion

To improve the *in vivo* characteristics the chelating moiety was modified with the amino acids Asn, Glu and Gla (γ-carboxyglutamic acid). Additionally, a precursor with triethyleneglycol as spacer between the piperazyl and quinolinyl moiety was synthesized to increase hydrophilicity of the underlying FAPI-29 without further modification at the chelating moiety. Compared to the initially synthesized ^{99m}Tc-FAPI-19 the derivatives ^{99m}Tc-FAPI-33 and -34 revealed higher uptake ratios of up to 45.8±1.3 % and 41.86±1.07 % on HT-1080-FAP cells (Fig. 2A). Furthermore, internalization rates above 95 % (Fig. 2A; Supplemental Table 2) and high affinity for FAP with IC_{50}-values of 10.9 nM (FAPI-33) and 6.9 (FAPI-34) were observed (Fig. 1) as evaluated by competition experiments (Fig. 2B). In contrast, less binding was measured for ^{99m}Tc-FAPI-27 (up to 12.94±0.77 %), -28 (up to 37.52±1.62 %), -29 (up to 39.34±1.01 %), and -43 (up to 28.83±0.88 %) after exposure to HT-1080-FAP cells for 4 h (Fig. 2A). Furthermore, competition experiments revealed a slightly reduced affinity of these derivatives for FAP with IC_{50} values of 12.0 nM (FAPI-29) and 12.7 nM (FAPI-28) (Fig. 1).

***In Vivo* Targeting Properties** and Pharmacokinetics **of ^{99m}Tc-labeled FAPI Derivatives**

^{99m}Tc-labeled FAPI tracers

To compare the *in vivo* targeting properties and pharmacokinetics of FAPI-28, -29, - 33, -34, and -43 with those of FAPI-19 planar scintigraphy and biodistribution experiments in HT-1080-FAP xenotranplanted mice were performed. The scintigraphic images demonstrated an improvement of the pharmacokinetics of the FAPI derivatives. Compared to FAPI-19 (Fig. 3A; Supplemental Fig. 3A) accumulation of radioactivity in the tumor lesion and reduction of the proportion of the hepatobiliary excretion was noticed 60 min lasting for at least 120 min after injection of the compounds (Fig. 3A). ^{99m}Tc-FAPI-34 showed the lowest uptake in the liver, biliary gland and the intestine **and a** significant uptake in tumor lesions of mice (Fig. 3A; Supplemental Fig. 3B) which was prevented by simultaneous injection of the unlabeled analog and confirmed the target specificity of the compound (Fig. 3B).

In accordance with these results, biodistribution experiments with ^{99m}Tc-FAPI-34 revealed a tumor uptake of 5.4±2.05 %ID/g and 4.3±1.95 %ID/g and liver uptake of 0.91±0.25 %ID/g and 0.73±0.18 %ID/g of 1 h and 4 h after injection of the tracer (Fig. 4A). Except for the kidneys, less than 1 %ID/g of the FAPI-34 activity was detected in the blood and organs of xenografts accounting for tumor-to-tissue ratios above one (Fig. 4B). In contrast, we measured a lower tumor uptake of ^{99m}Tc-FAPI-29 (2.79±1.19 %ID/g; 1.43±1.13 %ID/g) and of ^{99m}Tc-FAPI-43 (2.41±0.34 %ID/g; 2.57±0.32 %ID/g) 1 h and 4 h after tracer injection (Supplemental Fig. 4). The liver uptake of these derivatives, however, increased from 0.63±0.06 %ID/g to 1.73±1.33 %ID/g (FAPI-29) or slightly decreased from 1.74±0.28 %ID/g to 1.56±0.03 %ID/g (FAPI-43) after 1 h and 4 h. In summary, ^{99m}Tc-FAPI-34 provided the best pharmacokinetics in xenografts and was, therefore, clinically applied for scintigraphy/SPECT.

FAPI-34 Accumulates in Human Tumors

Two patients with metastasized ovarian and pancreatic cancer received PET with ^{68}Ga-FAPI-46, therapy with ^{90}Y-FAPI-46 in the setting of a last line treatment and scintigraphy/SPECT with ^{99m}Tc-FAPI-34. The patient with metastasized ovarian cancer had a ^{68}Ga-FAPI-46 PET/CT dated July 7 2018, followed by therapy with 6 GB ^{90}Y-FAPI-46 dated July 25 2018. Therapy follow up was done using ^{99m}Tc-FAPI-34

dated September 19 2018 showing stable disease. The patient with pancreatic cancer had a previous FAPI therapy in June 2018. The ^{99m}Tc-FAPI-34 scintigraphy was done for follow up. One day after scintigraphy another therapy was done with 6 GBq ^{90}Y-FAPI-46. Therapy was done with ^{90}Y because ^{188}Re was not available at this time. Six weeks later a follow up imaging was done with FAPI-46 PET/CT. In both cases the tumor lesions could be visualized (Figs. 5 and 6; Supplemental Figs. 5 and 6). Although in animal experiments evidence for a biliary secretion into the intestine was found, this was not the case in these patients.

DISCUSSION

The stromal component of tumors not only constitutes a major part of the tumor lesion, but is also involved in many stroma to tumor cell interactions such as signaling and remodeling of the extracellular matrix which may lead to immunosuppression, resistance to chemotherapy, angiogenesis, tumor growth and metastasis (*14-18*). Since cancer-associated fibroblasts (CAFs) are known as important drivers of these reactions, the development of targeting strategies against these cells can be useful for diagnostic as well as for therapeutic applications. In previous work we described a couple of tracers based on inhibitors of the fibroblast activation protein (*19,20*). These were conjugated to DOTA, enabling radiolabeling with a variety of commonly available radionuclides for PET imaging and possibly also for endoradiotherapy (*4-8,11*).

In order to optimize the efficacy of FAPI-based endoradiotheray the physical half-life of the therapeutic radionuclide used for labeling has to be adjusted to the tumor retention time. Since FAPIs show a faster elimination out of the tumor as compared to other molecules such as PSMA or somatostatin receptor ligands, ^{177}Lu or ^{225}Ac are not the ideal candidates for therapy with FAP inhibitors. In contrast, ^{188}Re, a beta emitter with a half-life of 17 h seems to be better suited. Therefore, FAPI variants with chelators dedicated for the binding of ^{99m}Tc and ^{188}Re were designed and evaluated *in vitro* and *in vivo*. Although all compounds displayed high affine FAP-specific binding with IC_{50} values ranging from 6.4 nM to 12.7 nM

and internalization of more than 95 %, small animal scintigraphy revealed different pharmacokinetic properties of the FAPI compounds Compared to the primary molecule FAPI-19 an improved tumor delineation was observed for FAPI-28, FAPI-29, FAPI-33, FAPI34 and FAPI-43. The high lipophilicity of tricarbonyl complex, as reported for PSMA ligands or somatostatin receptor targeted compounds (*21,22*), causes a hepatobiliary elimination of FAPI-19 resulting in a lack of tumor accumulation. This fact may result from an unspecific binding of blood components like lipoproteins, which overpowers the binding to FAP by inhibiting the conversion into the tumor tissue accompanied by a fast deposition rate in the liver without an enterohepatic circulation. However, as shown in Supplemental Table 1 all FAPI compounds revealed a comparable plasma protein binding. Furthermore, the attachment of amino acids with hydrophilic side chains results in only small reductions of the logP value. In case of arginine the difference was most noticeable, while the value counterintuitively was raised in a substance with additional polar groups, which also performed better than the original FAPI-19. Therefore, other factors must be responsible for the different tumor uptakes.

To enable renal excretion four derivatives with higher hydrophilicity were designed and evaluated. Due to the availability of the building blocks and their biocompatibility hydrophilic amino acids were chosen for the fine tuning of the radio tracers. A first tumor accumulation was achieved by the attachment of asparagine with a neutral carboxamide side chain (FAPI-28). However, the introduction of glutamic acid (FAPI-29) and, thereby, a negatively charged carboxylate side chain even improved tumor accumulation and renal clearance of the radiotracer. Since peritoneal metastases as well as liver cancers and metastases are important for diagnosis, the accumulation in intestine and liver had to be further minimized after enabling tumor targeting. Additionally, the slow hepatobiliary excretion would lead to a high non-target organ dose representing a major drawback for the envisaged therapy with ^{188}Re. Arginine (FAPI-43) with a positively charged residue was also tested but was discarded due to the slow background clearance in scintigraphy.

Due to the promising results with glutamic acid two alterations were tested to further improve the pharmacokinetic properties. One approach was the insertion of a triethyleneglycol linker and the other was the application of carboxyglutamic acid, which carries an additional negatively charged carboxyl function. The PEG derivative FAPI-33 showed similar tumor accumulation and biliary excretion to FAPI-29 with a supposedly longer circulation in the blood pool as a result of the expectable slower renal clearance caused by the higher hydrodynamic radius of PEG oligomers (*23*). In this series FAPI-29 and FAPI-34 were identified as the compounds with the lowest background activity in scintigraphy. Therefore, FAPI-29 and FAPI-34 were used for biodistribution studies. Although FAPI-34 showed a slower uptake *in vitro*, which might be caused by the two additional carboxyl functions, the *in vivo* performance of this compound in comparison to FAPI-29 could be improved. FAPI-34 revealed a stability in human serum over 4 hours without noticeable degradation products (Supplemental Fig.2), and a 2-fold and 8-fold higher tumor uptake at 1 h and 4 h p.i., respectively. Liver uptake was comparable at 1 h, but increased 2.7-fold for FAPI-29 at 4 h and remained stable for FAPI-34. Therefore, redistribution to the liver during hepatobiliary excretion with decreasing tracer availability to the tumor may be an explanation for the difference in tumor uptake. In view of the higher and constant tumor accumulation of FAPI-34 versus the lower and decreasing tumor uptake for FAPI-29 and the evidence obtained from the scintigraphy and biodistribution study for a hepatobiliary excretion for FAPI-29, FAPI-34 was chosen for application in humans.

However, a different kidney uptake in scintigraphy and biodistribution was observed. This may originate from resting activity in the urine of the pelvic system after sacrificing the animals i.e. a result of the difference between the in vivo situation in the small animal SPECT and the ex vivo situation during the biodistribution experiment. Consequently, the images obtained from two patients with metastasized cancer resemble better to the small animal PET with radioactivity seen predominantly in the renal pelvis as compared to the renal parenchyma, which was also observed with the ^{68}Ga-labeled FAPIs. The

scintigraphic images corresponded largely to the images obtained by PET/CT. However, we have to admit that the PET/CT was 8 weeks earlier and 5 weeks later than the SPECT/CT in the patient with ovarian cancer and the patient with the pancreatic cancer, respectively. This may be critical, especially in fastly growing tumors such as pancreatic and ovarian cancer and, therefore, requires additional patients where the time interval between PET/CT and SPECT is substantially shorter, i.e. 4 weeks at maximum.

Conclusion

Although all compounds displayed high affine FAP-specific binding with IC_{50} values ranging from 6.9 to 13 nM and internalization of more than 95 %, small animal scintigraphy revealed different pharmacokinetic properties of the FAPI derivatives. Compared to the primary compound FAPI-19 improved tumor delineation was observed for FAPI-19 derivatives which carry additional hydrophilic groups.

FAPI-34 may be a good candidate for scintigraphic imaging due to its high contrast obtained by rapid tumor uptake and fast clearance from the rest of the body. Since the chelator allows labeling with ^{188}Re, the tracer may also be applicable for endoradiotherapy of desmoplastic tumors with high FAP expression. However, this has to be shown with data obtained in more patients and of course requires dosimetric calculations.

Acknowledgements

The authors gratefully acknowledge Stefan Bauer (National Center for Tumor Diseases, Heidelberg) for supplying the FAP-α and CD26 transfected cell lines. The authors thank Stephanie Biedenstein, Kirsten Kunze, Irina Kupin, Vanessa Kohl, Marlene Tesch and Karin Leotta for excellent technical assistance. This work was funded in part by the Federal Ministry of Education and Research, grant number 13N 13341.

DISCLOSURE STATEMENT

Patent application for Anastasia Loktev, Thomas Lindner, Walter Mier, Clemens Kratochwil, Frederik Giesel and Uwe Haberkorn. No other potential conflicts of interest relevant to this article exist.

Key Points

QUESTION: To establish a FAPI variant which can be used for scintigraphy and ^{188}Re endoradiotherapy.

PERTINENT FINDINGS: The systematic variation of the linker and chelator resulted in a SPECT tracer with high tumor uptake and low background in animals as well as in first patient examinations.

IMPLICATIONS FOR PATIENT CARE: the new variant FAPI-34 shows promise for scintigraphic visualization and endoradiotherapy of FAP-positive tumors.

References

1. Marsh T, Pietras K, McAllister SS. Fibroblasts as architects of cancer pathogenesis. *Biochimica et biophysica acta.* 2013;1832:1070-1078.

2. Lamprecht S, Sigal-Batikoff I, Shany S, et al. Teaming Up for Trouble: Cancer Cells, Transforming Growth Factor-β1 Signaling and the Epigenetic Corruption of Stromal Naïve Fibroblasts. *Cancers.* 2018;10:61.

3. Jiang G-M, Xu W, Du J, et al. The application of the fibroblast activation protein α-targeted immunotherapy strategy. *Oncotarget.* 2016;7:33472-33482.

4. Loktev A, Lindner T, Mier W, et al. A Tumor-Imaging Method Targeting Cancer-Associated Fibroblasts. *J Nucl Med.* 2018;59:1423-1429.

5. Lindner T, Loktev A, Altmann A, et al. Development of Quinoline-Based Theranostic Ligands for the Targeting of Fibroblast Activation Protein. *J Nucl Med.* 2018;59:1415-1422.

6. Kratochwil C, Flechsig P, Lindner T, et al. (68)Ga-FAPI PET/CT: Tracer Uptake in 28 Different Kinds of Cancer. *J Nucl Med.* 2019;60:801-805.

7. Giesel F, Kratochwil C, Lindner T, et al. FAPI-PET/CT: biodistribution and preliminary dosimetry estimate of two DOTA-containing FAP-targeting agents in patients with various cancers. *J Nucl Med.* 2018.

8. Giesel FL, Heussel CP, Lindner T, et al. FAPI-PET/CT improves staging in a lung cancer patient with cerebral metastasis. *Eur J Nucl Med Mol Imaging.* 2019;46:1754-1755.

9. Lindner T, Loktev A, Giesel F, Kratochwil C, Altmann A, Haberkorn U. Targeting of activated fibroblasts for imaging and therapy. *EJNMMI Radiopharmacy and Chemistry.* 2019;4:16.

10. Zimmerman CN, Babich JW, Joyal JL, Marquis JC, Wang J-C, Zimmerman CN, Babich JW, Joyal JL, Marquis JC, Wang J-CZimmerman CN, Babich JW, Joyal JL, Marquis JC, Wang J-Cs. Selective Seprase Inhibitors. US patent US20100098633A1, 2009.

11. Loktev A, Lindner T, Burger EM, et al. Development of novel FAP-targeted radiotracers with improved tumor retention. *J Nucl Med.* 2019.

12. Fischer E, Chaitanya K, Wuest T, et al. Radioimmunotherapy of fibroblast activation protein positive tumors by rapidly internalizing antibodies. *Clin Cancer Res.* 2012;18:6208-6218.

13. Kelly T. Fibroblast activation protein-alpha and dipeptidyl peptidase IV (CD26): cell-surface proteases that activate cell signaling and are potential targets for cancer therapy. *Drug Resist Updat.* 2005;8:51-58.

14. Plava J, Cihova M, Burikova M, Matuskova M, Kucerova L, Miklikova S. Recent advances in understanding tumor stroma-mediated chemoresistance in breast cancer. *Mol Cancer.* 2019;18:67.

15. Pure E, Lo A. Can Targeting Stroma Pave the Way to Enhanced Antitumor Immunity and Immunotherapy of Solid Tumors? *Cancer Immunol Res.* 2016;4:269-278.

16. Bussard KM, Mutkus L, Stumpf K, Gomez-Manzano C, Marini FC. Tumor-associated stromal cells as key contributors to the tumor microenvironment. *Breast Cancer Res.* 2016;18:84.

17. Erdogan B, Webb DJ. Cancer-associated fibroblasts modulate growth factor signaling and extracellular matrix remodeling to regulate tumor metastasis. *Biochem Soc Trans.* 2017;45:229-236.

18. Gascard P, Tlsty TD. Carcinoma-associated fibroblasts: orchestrating the composition of malignancy. *Genes Dev.* 2016;30:1002-1019.

19. Jansen K, Heirbaut L, Cheng JD, et al. Selective Inhibitors of Fibroblast Activation Protein (FAP) with a (4-Quinolinoyl)-glycyl-2-cyanopyrrolidine Scaffold. *ACS medicinal chemistry letters.* 2013;4:491-496.

20. Jansen K, Heirbaut L, Verkerk R, et al. Extended Structure–Activity Relationship and Pharmacokinetic Investigation of (4-Quinolinoyl)glycyl-2-cyanopyrrolidine Inhibitors of Fibroblast Activation Protein (FAP). *Journal of Medicinal Chemistry.* 2014;57:3053-3074.

21. Lu G, Maresca KP, Hillier SM, et al. Synthesis and SAR of 99mTc/Re-labeled small molecule prostate specific membrane antigen inhibitors with novel polar chelates. *Bioorganic & Medicinal Chemistry Letters.* 2013;23:1557-1563.

22. Maresca KP, Marquis JC, Hillier SM, et al. Novel Polar Single Amino Acid Chelates for Technetium-99m Tricarbonyl-Based Radiopharmaceuticals with Enhanced Renal Clearance: Application to Octreotide. *Bioconjugate Chemistry.* 2010;21:1032-1042.

23. Kang JS, DeLuca PP, Lee KC. Emerging PEGylated drugs. *Expert Opinion on Emerging Drugs.* 2009;14:363-380.

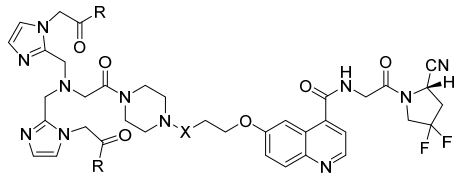

Name	X =	R =	IC_{50} [nM]
FAPI-19	-CH_2-	-OH	6.4
FAPI-28	-CH_2-	-L-Asn	12.7
FAPI-29	-CH_2-	-*N*-L-Glu	12.0
FAPI-33	-$(C_2H_4O)_2$-	-*N*-L-Glu	10.9
FAPI-34	-CH_2-	-*N*-L-Gla	6.9
FAPI-43	-CH_2-	-*N*-D-Arg	n.d.

Figure 1. FAPI-derivatives for ^{99m}Tc-labeling and corresponding IC_{50}-values.

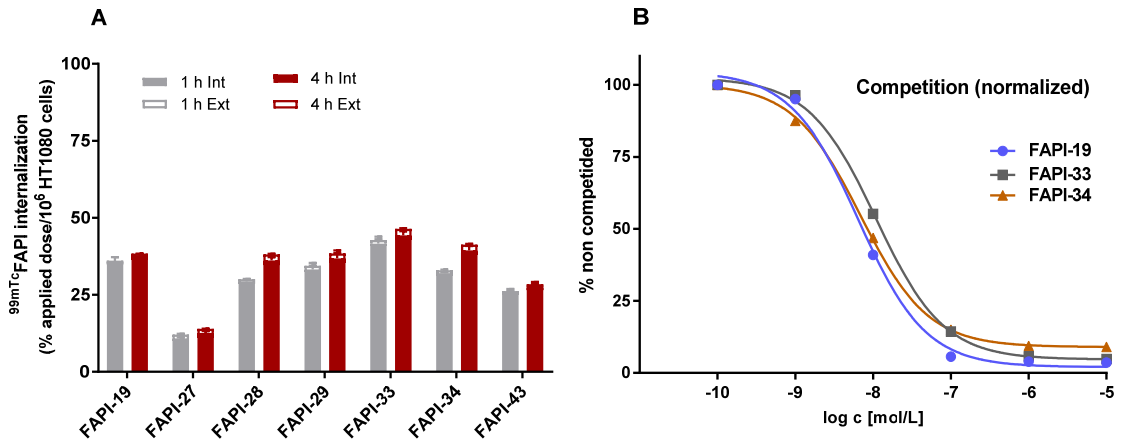

Figure 2. A Binding of ^{99m}Tc-labeled FAPI-19, -28, -29, -33, -34, and -43 to HT-1080-FAP. B Competitive binding of radiolabeled FAPI-19, FAPI-33 and FAPI-34 to HT-1080-FAP cells after adding increasing concentrations of the corresponding unlabeled FAPIs. All values are given as percentage of total applied dose normalized to 1 million cells (%ID/1 x 10^6 cells).

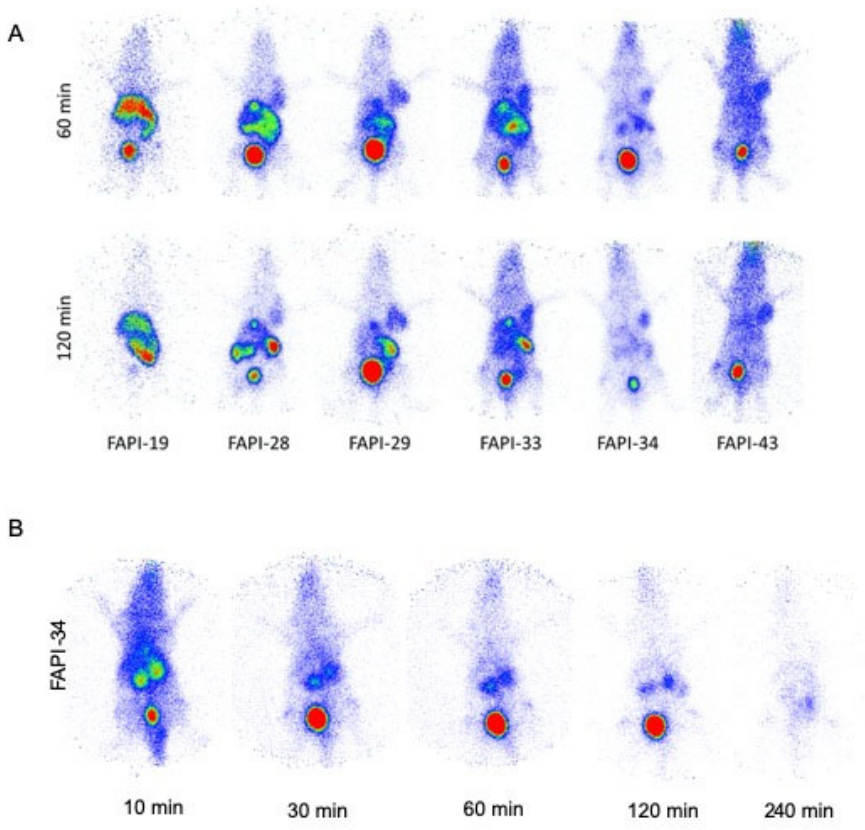

Figure 3. Planar scintigraphy of HT-1080-FAP tumor bearing nude mice (A) 60 min and 120 min after application of ^{99m}Tc-labeled FAPI-derivatives and (B) 10 min, 30 min, 1 h, 2 h, and 4 h after simultaneous injection of 30nmol unlabeled FAPI-34 used as competitor and ^{99m}Tc-FAPI-34. Images are collected over 10 min at the individual time points.

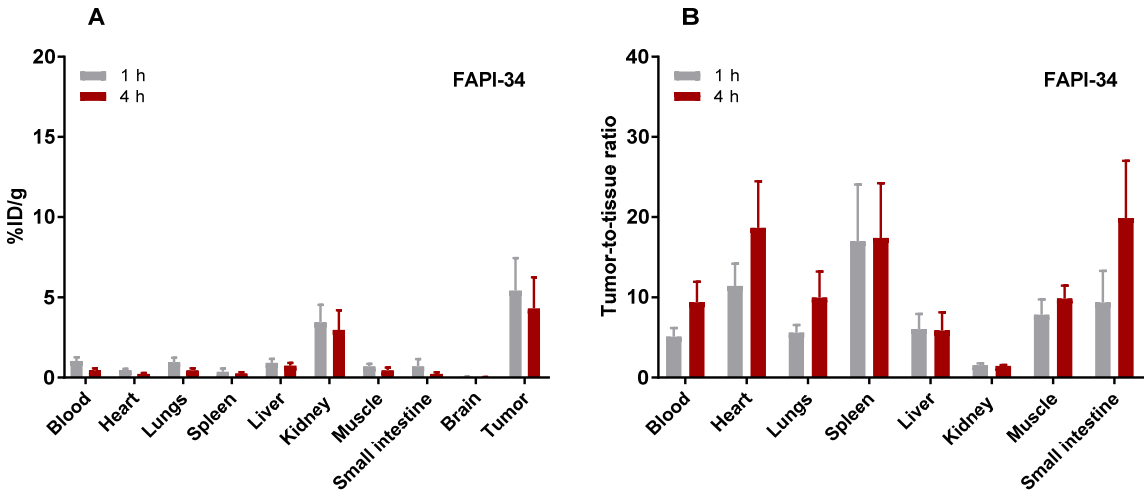

Figure 4. (A) Biodistribution of ^{99m}Tc-FAPI-34 in HT-1080-FAP xenotransplanted mice and (B) tumor-to-tissue ratios 1 h and 4 h after application of the radiotracer. N=6 for each time point. The values stated are expressed as percentage of injected dose per gram of tissue (%ID/g).

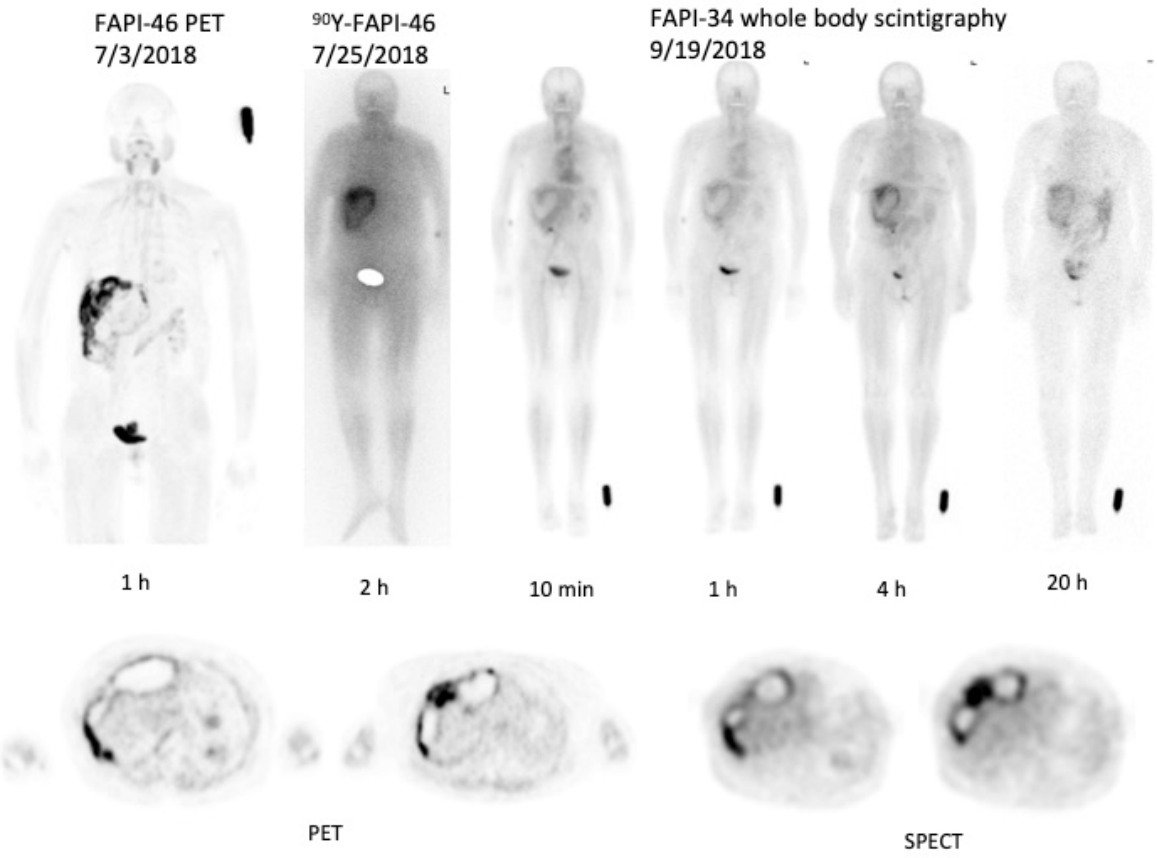

Figure 5. ^{68}Ga-FAPI-46 PET/CT (*11*), intratherapeutic imaging (Bremsstrahlung) during treatment with 6 GBq ^{90}Y-FAPI-46 and scintigraphy with ^{99m}Tc-labeled FAPI-34 (planar scintigraphy and transaxial SPECT slices) in a patient with ovarian cancer.

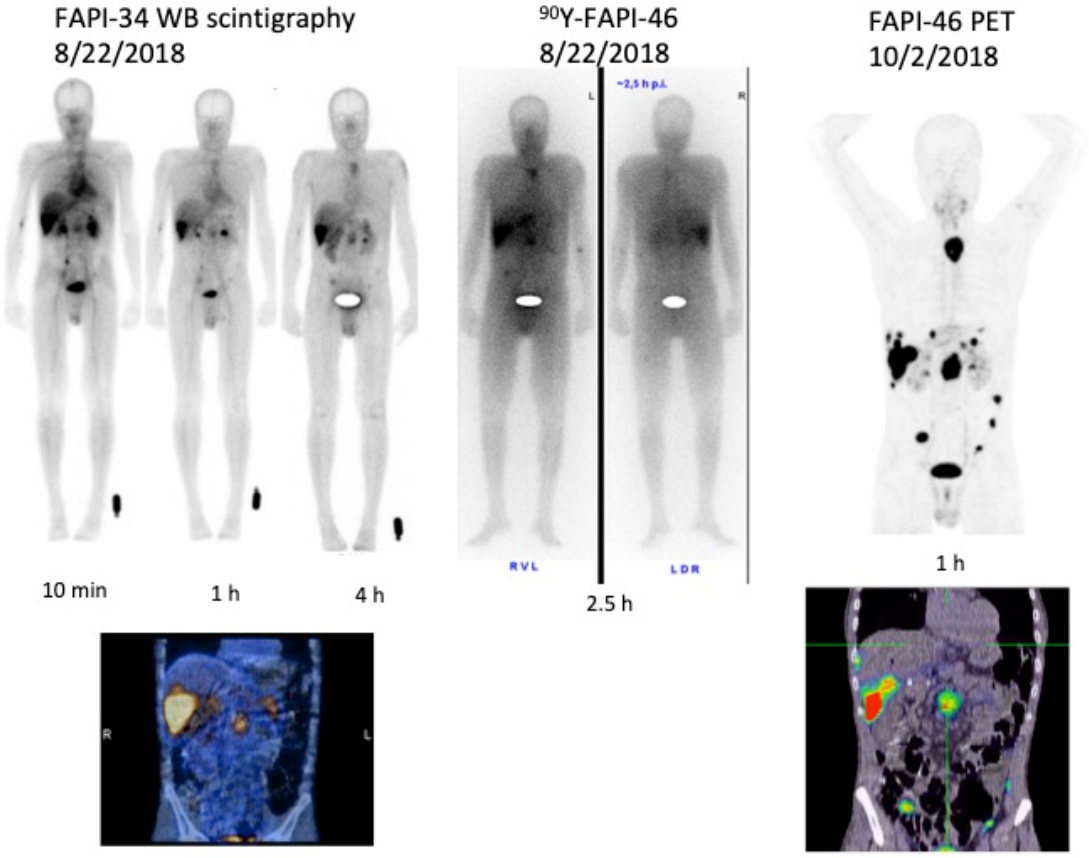

Figure 6. ^{99m}Tc-labeled FAPI-34 in planar scintigraphy and coronal SPECT fusion slides intratherapeutic imaging (Bremsstrahlung) during treatment with 6 GBq ^{90}Y-FAPI-46 and ^{68}Ga-labeled FAPI-46 PET-imaging (*11*) in a patient with pancreatic cancer.

Supporting Information

Reagents

All solvents and non-radioactive reagents were obtained in reagent grade from ABCR (Karlsruhe, Germany), Sigma-Aldrich (München, Germany), Acros Organics (Geel, Belgium) or VWR (Bruchsal, Germany) and were used without further purification. (*S*)-*N*-(2-(2-cyano-4,4-difluoropyrrolidin-1-yl)-2-oxoethyl)-6-(3-(4-*tert*-butoxycarbonylpiperazin-1-yl)-1-propoxy)quinoline-4-carboxamide was synthesized as already described (*1*). The chelator bis((1-(2-(tert-butoxy)-2-oxoethyl)1H-imidazol-2-yl)methyl)glycine was synthesized according to Lu et al.(*2*) using hydrogen over 5% Pd/C in methanol for the reductive amination step. Technetium (Tc-99m) was eluted from a Mo-99/Tc-99m generator purchased from CIS bio GmbH (Berlin, Germany). Human serum was obtained from Sigma-Aldrich (München, Germany).

Compound Synthesis

Supplemental Figure 1 depicts the synthesis of FAPI-19 and the route to the following derivatives.

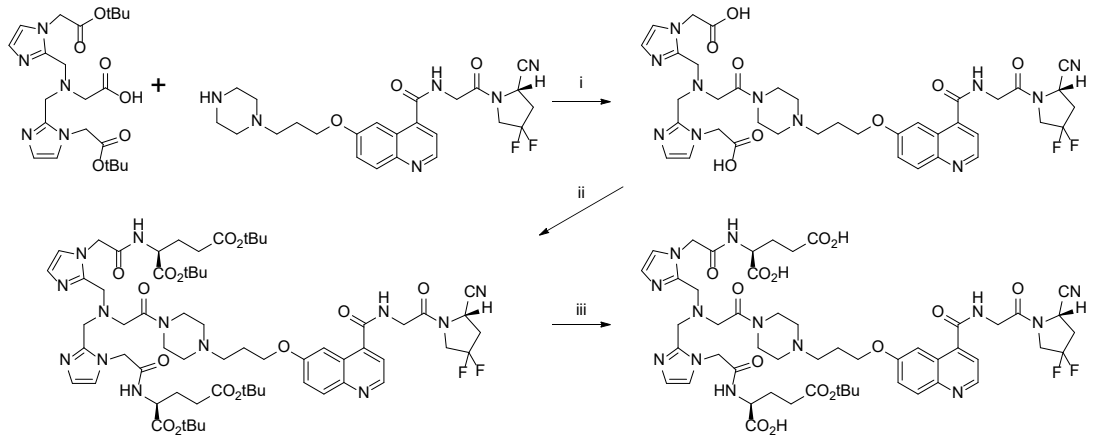

Supplemental Figure 1. Exemplary synthesis of FAPI-29 via FAPI-19. i) HBTU, HOBt, DIPEA then 2.5% TfOH in TFA/MeCN 4:1; ii) HBTU, HOBt, DIPEA, H-Glu(tBu)-OtBu; iii) 2.5% TfOH in TFA/MeCN 4:1.

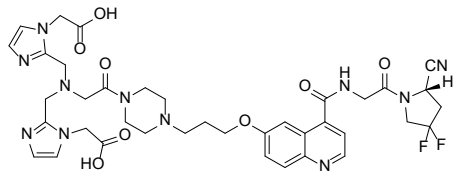

FAPI-19

1.09 mg (1.86 µmol) of (*S*)-*N*-(2-(2-cyano-4,4-difluoropyrrolidin-1-yl)-2-oxoethyl)-6-(3-(4-*tert*-butoxycarbonylpiperazin-1-yl)-1-propoxy)quinoline-4-carboxamide were treated with 100 µL

trifluoroacetic acid/acetonitrile 4:1 for 15 min and precipitated after removal of the solvents. The precipitate was reacted with 2.74 mg (5.91 µmol) bis((1-(2-(*tert*-butoxy)-2-oxoethyl)-1H-imidazol-2-yl)methyl)glycine, 2.13 mg (5.62 µmol) HBTU and 2.5 µL DIPEA in 150 µL dimethylformamide. After HPLC purification and solvent removal the residue was treated with 200 µL of 2.5% trifluoromethanesulfonic acid in trifluoroacetic acid/acetonitrile 4:1. After precipitation with diethyl ether and HPLC purification 1.06 mg (1.29 µmol; 70%) of the title compound were obtained.

LC-MS R_t 8.91 min, m/z 820.2933 $[M+H]^+$

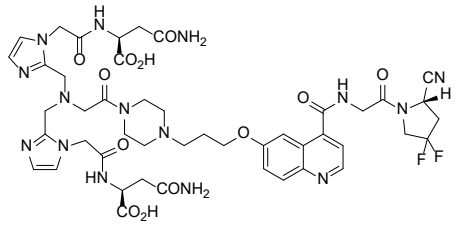

FAPI-28

1 µL (0.74 mg; 5.73 µmol) DIPEA was added to a solution of 0.95 mg (1.16 µmol) FAPI-19, 0.42 mg (3.14 µmol) HOBt and 1.10 mg (2.89 µmol) HBTU in 50 µL DMF. After 10 min 2.30 mg (5.34 µmol) H-Asn(Trt)-OtBu were added and reacted for 120 min. The *tert*-butyl protecting groups were removed by 100 µL 2.5% trifluoromethanesulfonic acid in trifluoroacetic acid/acetonitrile 4:1 after HPLC-purification and freeze-drying. 0.79 mg (0.75 µmol; 65%) were obtained after a final HPLC-purification and freeze-drying.

LC-MS R_t 9.23 min, m/z 524.7100 $[M+2H]^{2+}$

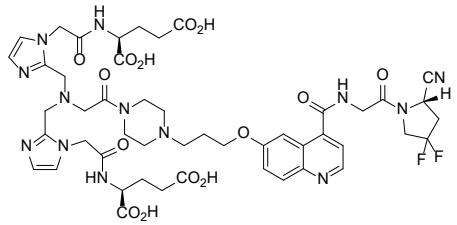

FAPI-29

0.81 mg (0.75 µmol; 65%) were obtained analogous to FAPI-28.

LC-MS R_t 9.25 min, m/z 1078.4109 $[M+H]^+$

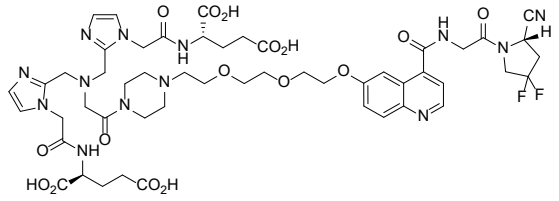

FAPI-33

0.64 mg (0.55 µmol; 60%) were obtained analogous to FAPI-28.

LC-MS R_t 9.85 min, m/z 1152.4493 $[M+H]^+$

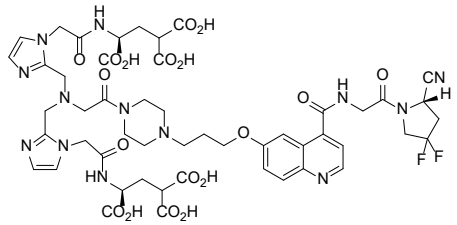

FAPI-34

1.01 mg (0.87 µmol; 52%) were obtained analogous to FAPI-28.

LC-MS R_t 8.87 min, m/z 583.6988 $[M+2H]^{2+}$

Compound Analysis

Reverse-phase high-performance liquid chromatography (RP-HPLC) was conducted using linear gradients of acetonitrile in water (0-100% acetonitrile in 5 min; 0.1 % TFA; flowrate 2 mL/min) on a Chromolith Performance RP-18e column (100 × 3 mm; Merck KGaA Darmstadt, Germany). UV-absorbance was detected at 214 nm. An additional γ-detector was used for the HPLC-analysis of radioactive compounds. HPLC-MS characterization was performed on an ESI mass spectrometer (Exactive, Thermo Fisher Scientific, Waltham, MA, USA) connected to an Agilent 1200 HPLC system with a Hypersil Gold C18 1.9 µm column (200 × 2.1 mm; 0-100 % acetonitrile in 20 min; flowrate 200 µL/min). Analytical Radio-HPLC was performed using a Chromolith Performance RP-18e column (100 × 3mm; Merck; 0-30 % acetonitrile in 10 min; flowrate 2 mL/min). HPLC-purifications were performed on a LaPrep P110-System (Knauer, Berlin, Germany) and a Reprosil Pur 120 column (C18-aq 5 µm 250 × 25mm; Dr. Maisch, Ammerbuch-Entringen, Germany). The water/acetonitrile-gradient (15 or 25 min; 0.1 % TFA; flowrate 20 mL/min) was modified for the individual products.

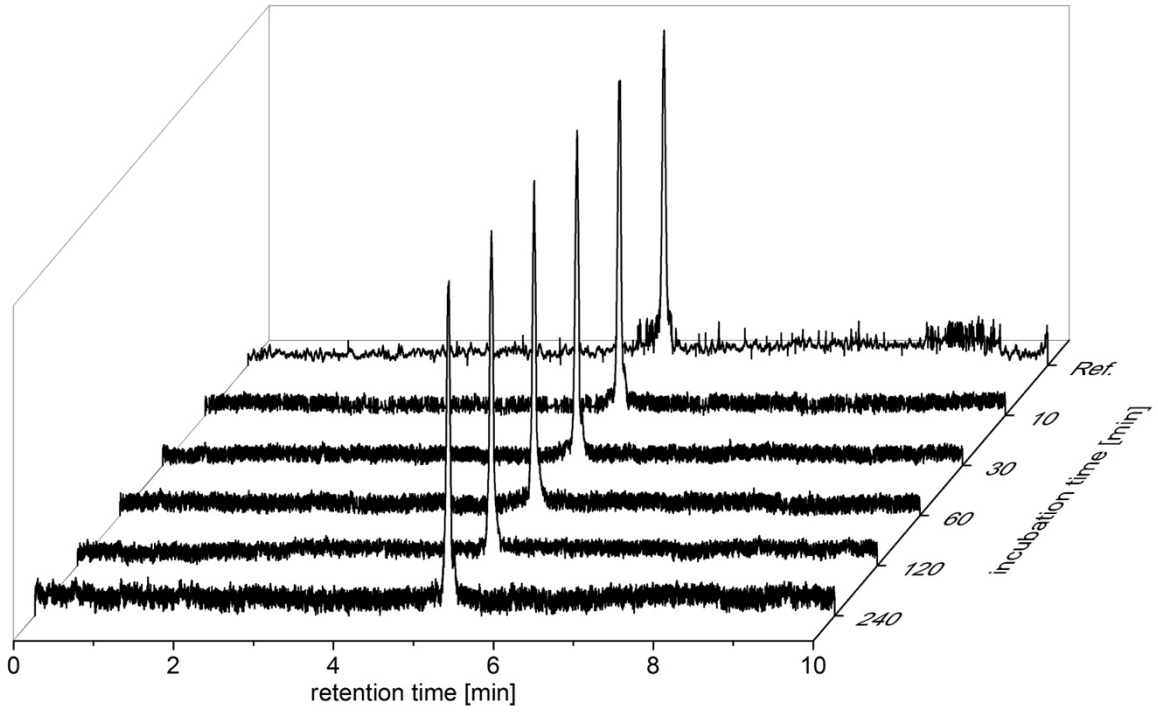

Supplemental Figure 2: Stability of ^{99m}Tc-FAPI-34 in human serum. Samples were precipitated after the indicated time points and the supernatant subjected to radio-HPLC analysis using a linear gradient from 0 to 50 % acetonitrile, containing 0.1 % TFA over 10 min. Neither free radioactivity nor peaks with different retention time than the reference peak were observed confirming the stability against degradation in human serum.

	logP	percent protein bound
^{99m}Tc-FAPI-19	**-1.48**	**96**
^{99m}Tc-FAPI-28	**-1.68**	**97**
^{99m}Tc-FAPI-29	**-1.68**	**97**
^{99m}Tc-FAPI-33	**-1.60**	**95**
^{99m}Tc-FAPI-34	**-1.54**	**98**
^{99m}Tc-FAPI-43	**-1.13**	**98**

Supplemental Table 1. The pharmacokinetic parameter plasma protein binding was determined by ultrafiltration (Amicron Ultra 0.5 mL; 10 kDa) of a serum sample incubated with the radioactive tracer followed by measurement of the radioactivity in the filtrate and the spinfilter. The physicochemical parameter log P were determined for a selection of six technetium labeled compounds following the procedure of Wilson *et al*. (*3*).

%AD/10^6 cells	Cell-bound fraction (1 h)	Internalized fraction (1 h)	Cell-bound fraction (4 h)	Internalized fraction (4 h)
FAPI-19	0.54±0.02	35.59±1.68	0.54±0.01	37.81±0.39
FAPI-27	1.23±0.23	10.9±0.25	1.34±0.02	12.65±0.62
FAPI-28	0.76±0.03	29.37±0.5	1.9±0.22	36.2±1.05
FAPI-29	1.16±0.09	33.26±2.14	1.6±0.12	36.9±2.56
FAPI-33	1.16±0.26	41.65±2.21	2.13±0.19	44.33±1.32
FAPI-34	0.94±0.14	32.07±0.33	1.86±0.23	39.47±1.4
FAPI-43	0.43±0.04	25.77±1.12	0.46±0.03	28.05±1.14

Supplemental Table 2. Cell-bound (glycin fraction) and internalized activity (lysed fraction) of HT-1080-FAP cells exposed to ^{99m}Tc labeled FAPI derivatives for 1 h and 4 h (%AD/10^6 cells+SD).

FAPI-19 %AD/10^6cells	10 min	60 min
HEK-muFAP	26.13±0.84	36.13±2.23
HEKCD26	0.13±0.01	0.19±0.02

Supplemental Table 3. Binding of ^{99m}Tc-FAPI-19 against HEK cells transfected with murine FAP (HEK-muFAP) or human CD26 (HEKCD26).

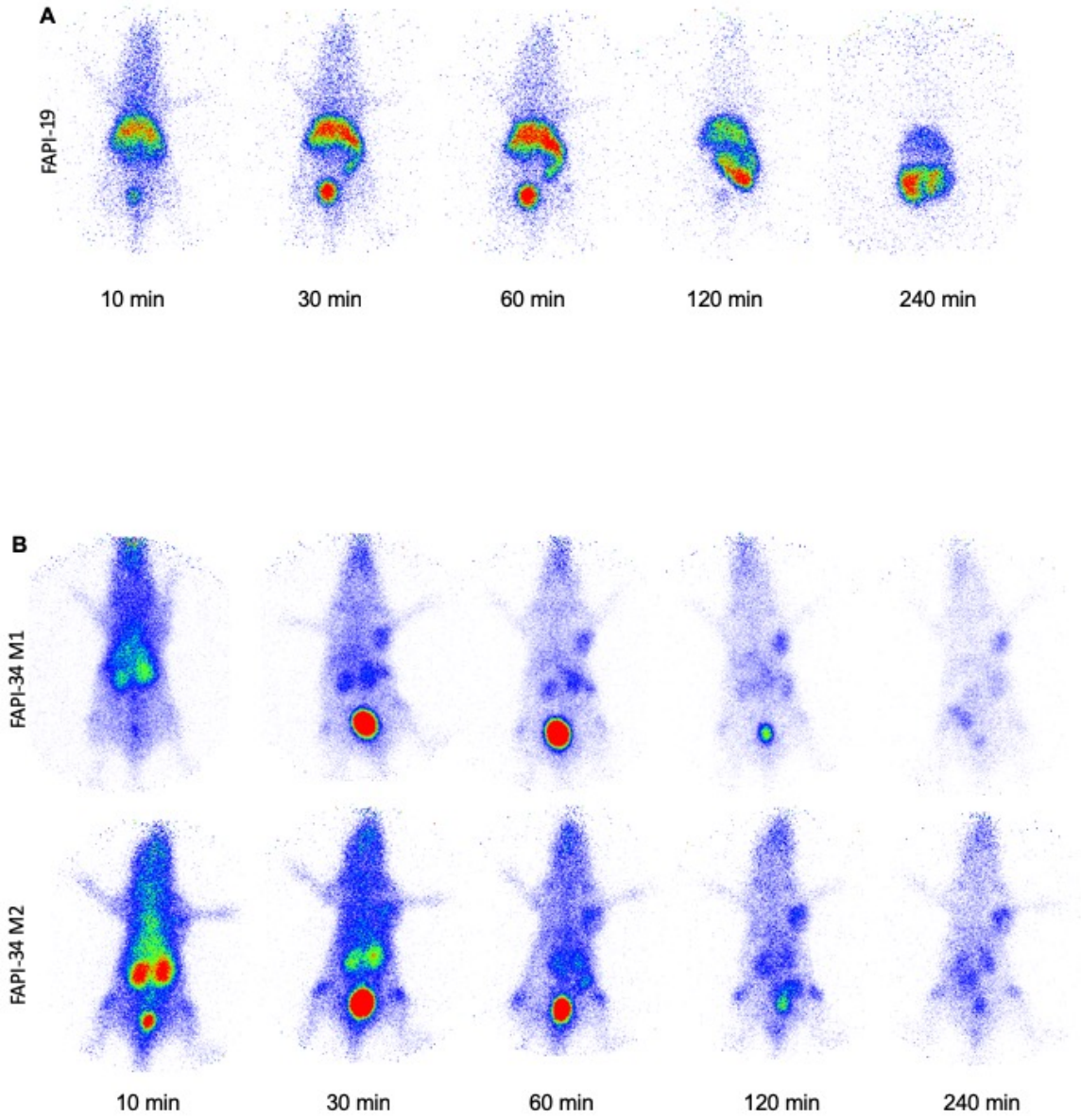

Supplemental Figure 3. Time course of planar scintigraphy with ^{99m}Tc-labeled (A) FAPI-19 and (B) FAPI-34 (two mice) in HT-1080-FAP xenotransplanted mice.

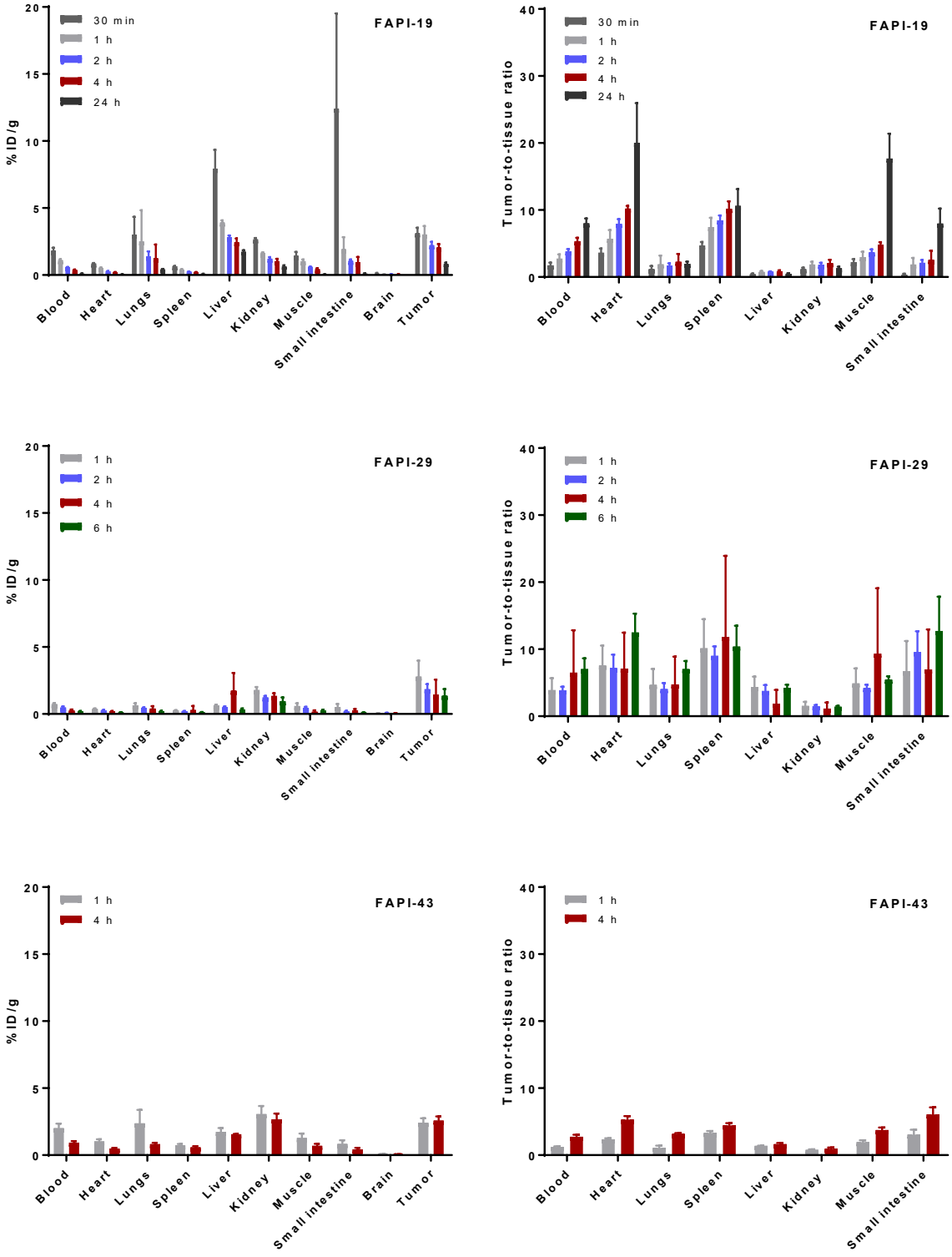

Supplemental Figure 4: Biodistribution (%ID/g; left) and Tumor-to-tissue ratios (right) of ^{99m}Tc-labeled FAPI-19, -29, and -43 (n=3).

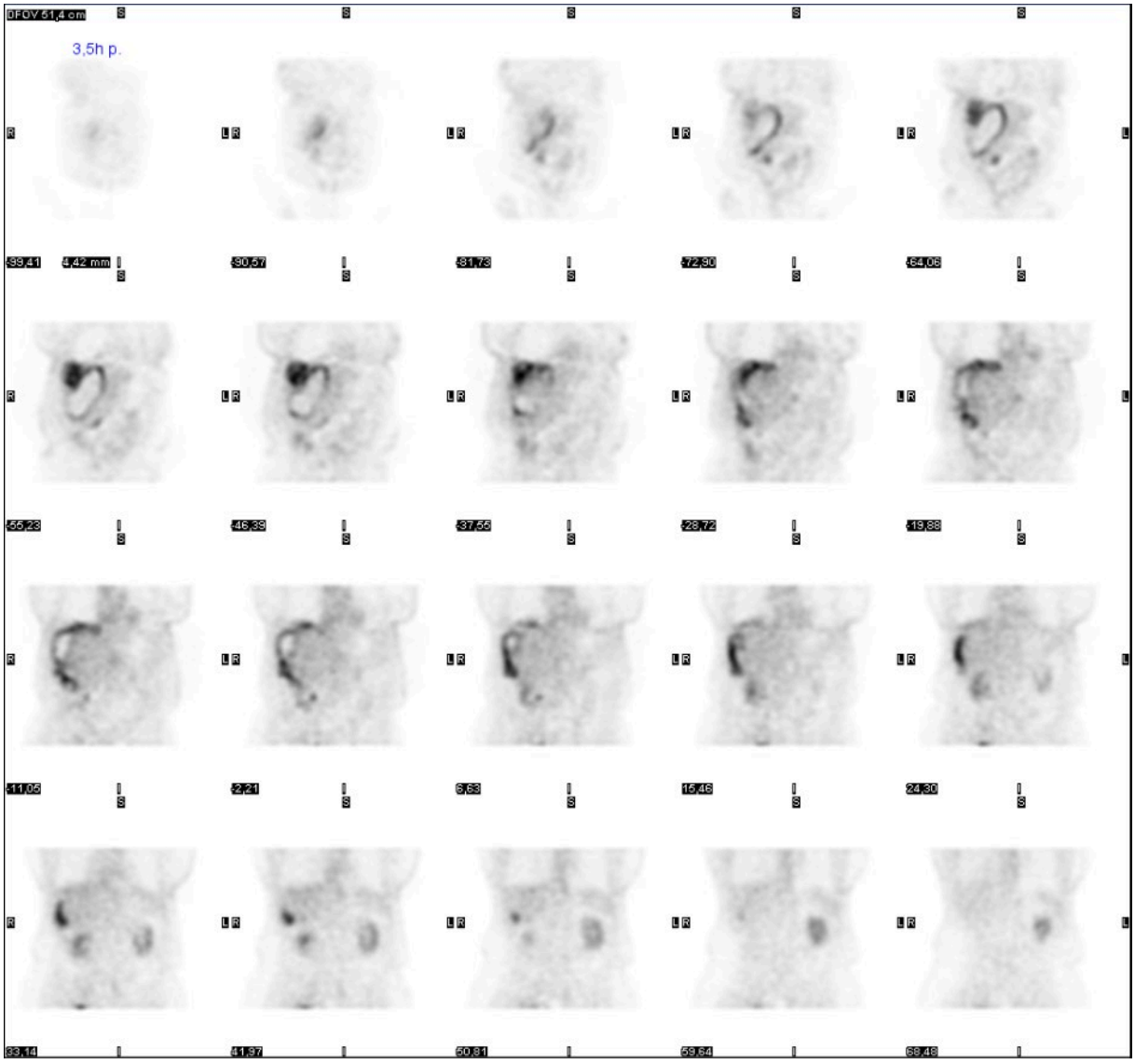
DFOV 51,4 cm
3,5h p.
-99,41
4,42 mm
-90,57
-81,73
-72,90
-64,08
-56,23
-46,39
-37,56
-28,72
-19,88
-11,05
-2,21
6,63
15,46
24,30
33,14
41,97
50,81
59,64
68,48

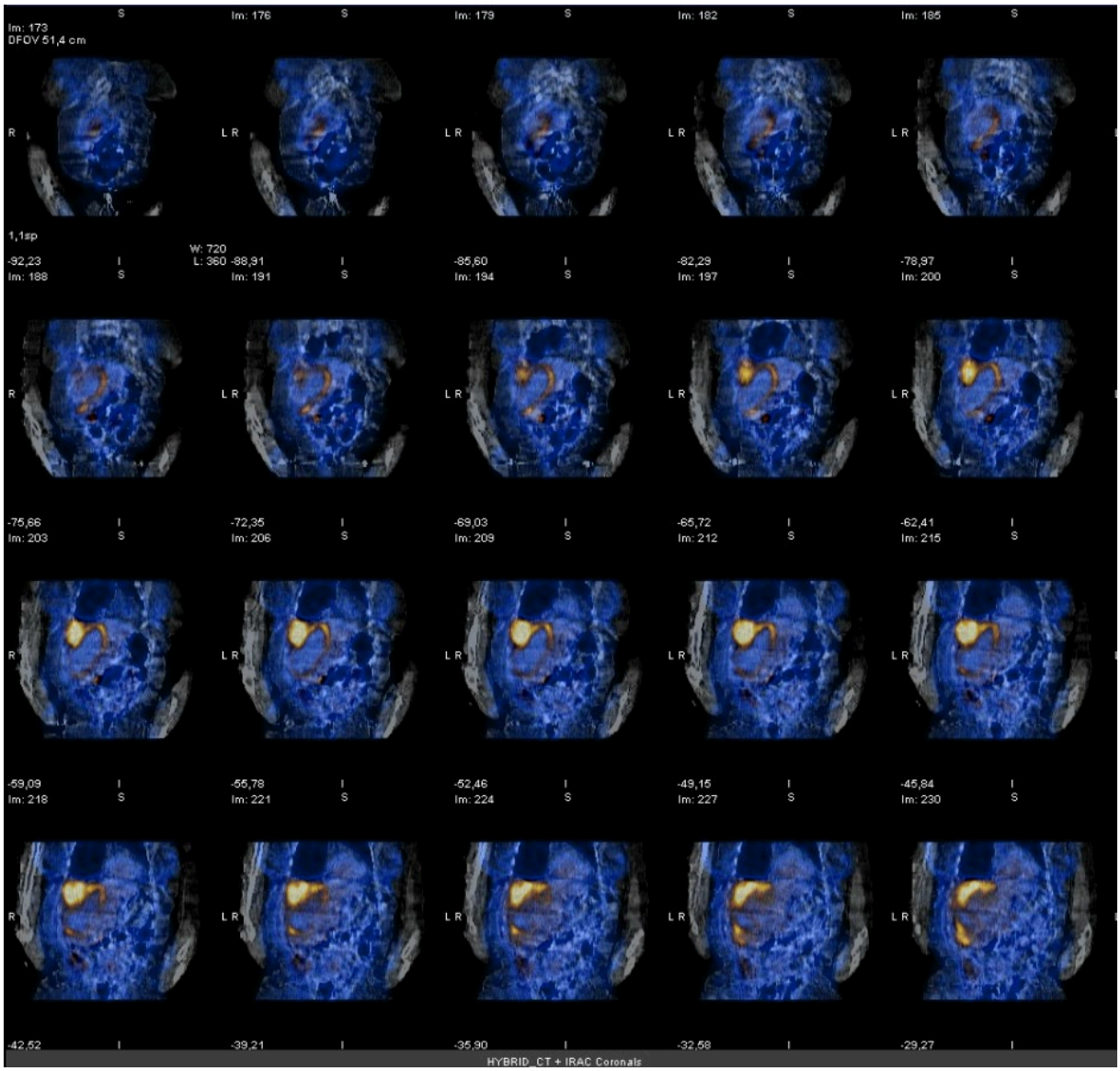
Im: 173
DFOV 51,4 cm
Im: 176
Im: 179
Im: 182
Im: 185
1,1sp
W: 720
L: 360
-92,23
Im: 188
-88,91
Im: 191
-85,60
Im: 194
-82,29
Im: 197
-78,97
Im: 200
-75,66
Im: 203
-72,35
Im: 206
-69,03
Im: 209
-65,72
Im: 212
-62,41
Im: 215
-59,09
Im: 218
-55,78
Im: 221
-52,46
Im: 224
-49,15
Im: 227
-45,84
Im: 230
-42,52
-39,21
-35,90
-32,58
-29,27
HYBRID_CT + IRAC Coronals

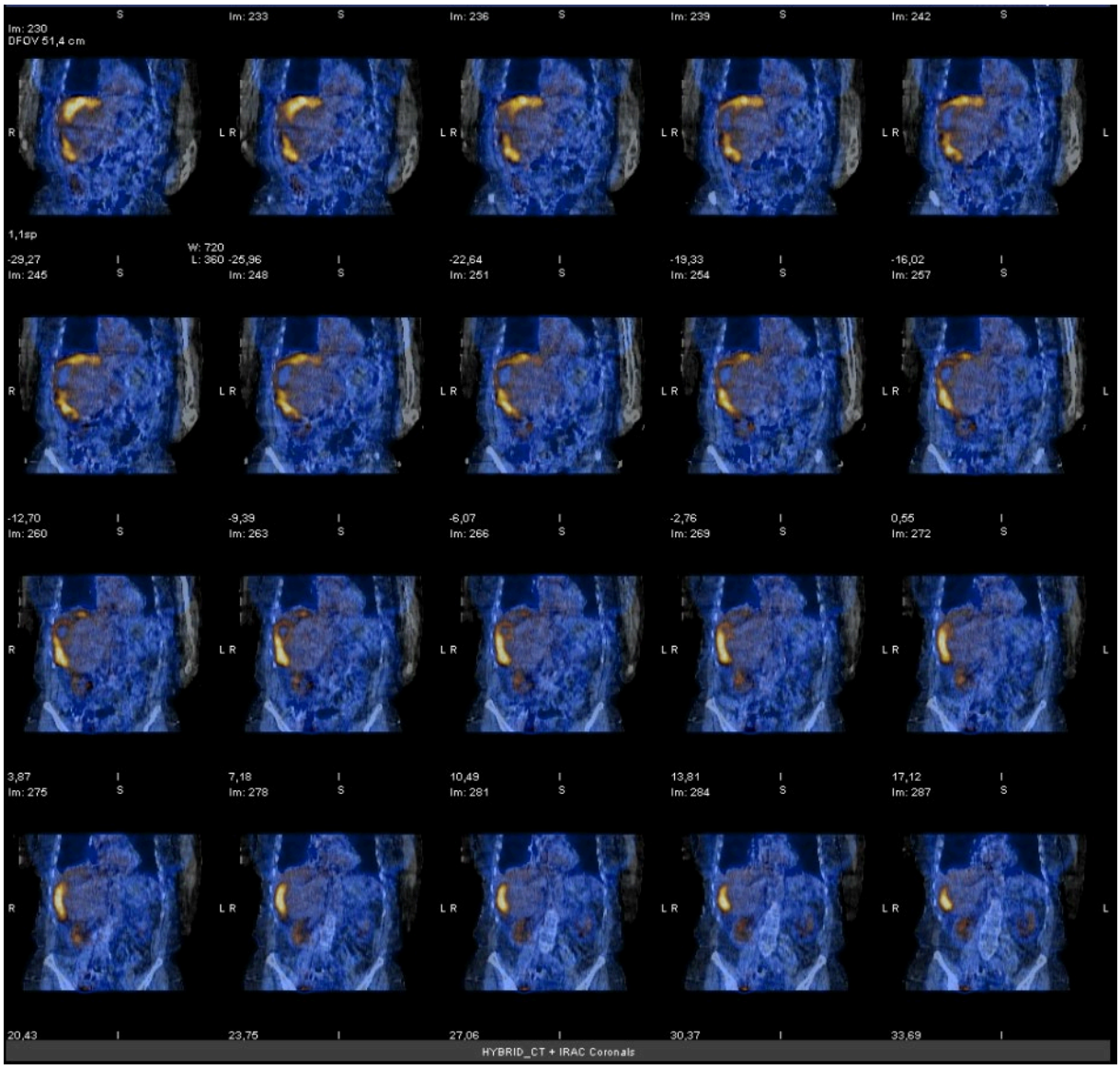

Supplemental Figure 5: Coronal SPECT and fusion SPECT/CT images of the patient with ovarian cancer presented in Figure 5.

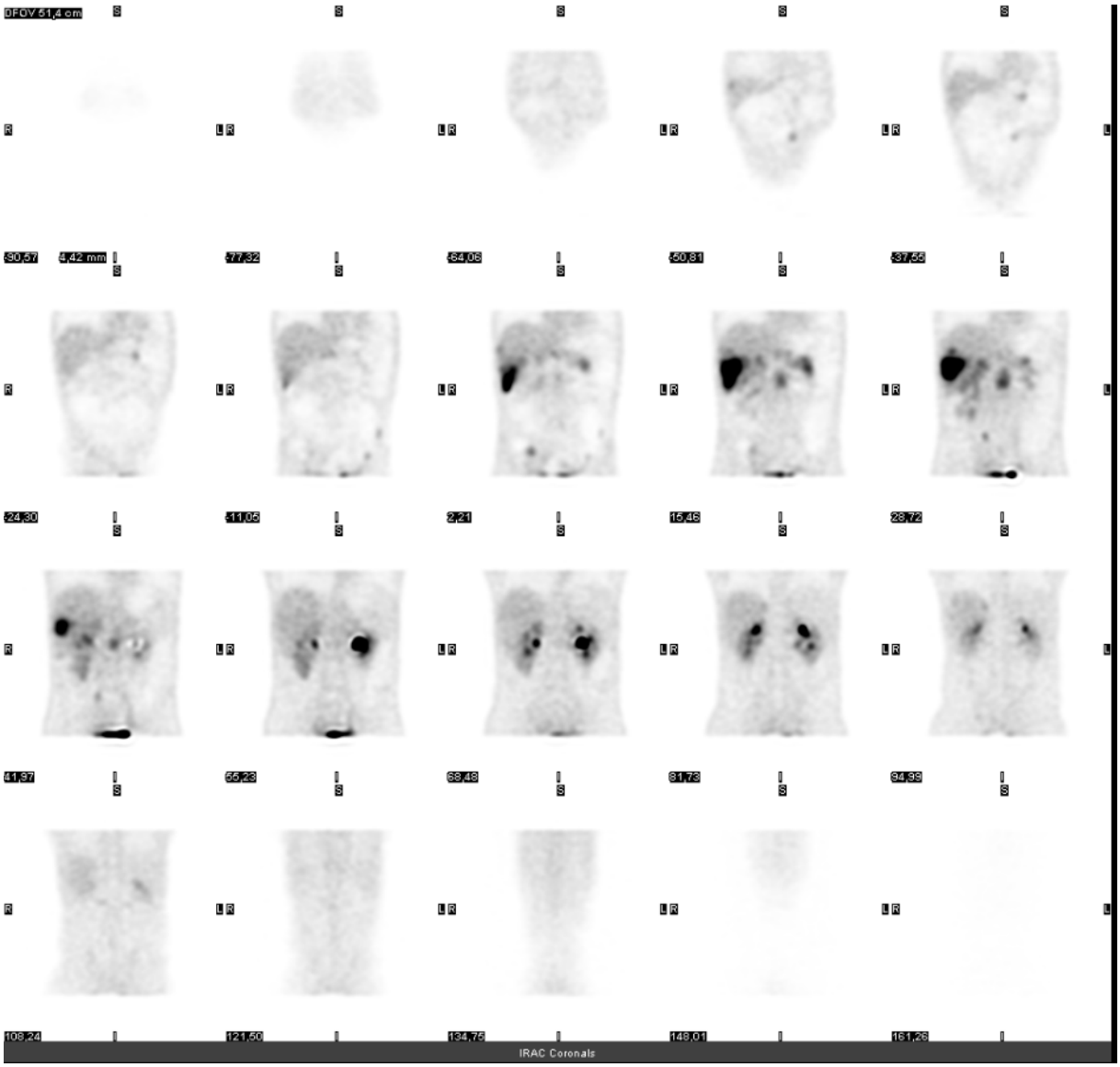
DFOV 51,4 cm
-30,57
4,42 mm
-77,32
-64,06
-50,81
-37,55
-24,30
-11,06
2,21
15,46
28,72
41,97
55,23
68,48
81,73
94,99
108,24
121,50
134,75
148,01
161,26
IRAC Coronals

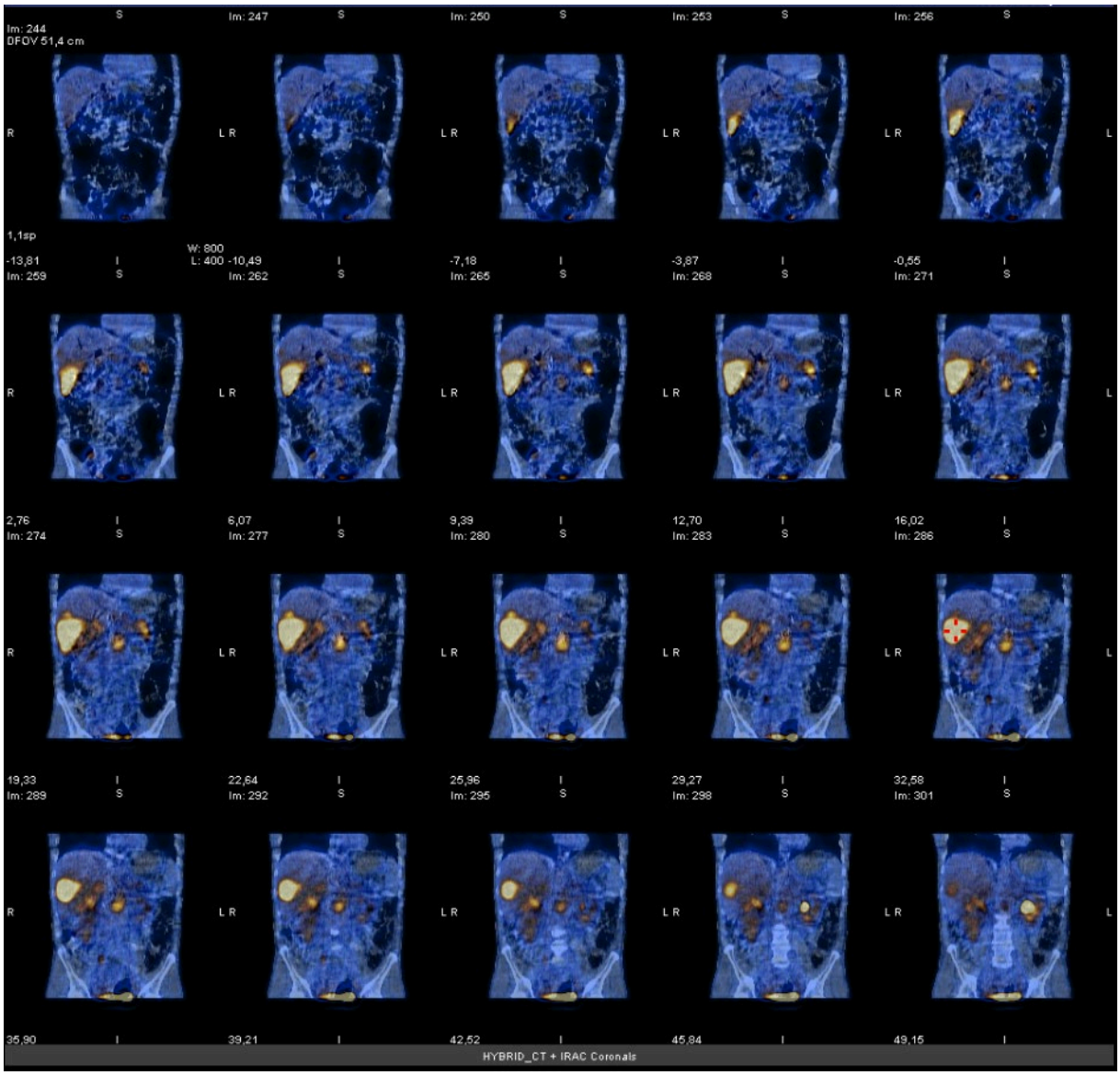

Supplemental Figure 6: Coronal SPECT and fusion SPECT/CT images of the patient with pancreatic cancer presented in Figure 6.

1. Lindner T, Loktev A, Altmann A, et al. Development of Quinoline-Based Theranostic Ligands for the Targeting of Fibroblast Activation Protein. *J Nucl Med.* 2018;59:1415-1422.

2. Lu G, Maresca KP, Hillier SM, et al. Synthesis and SAR of (9)(9)mTc/Re-labeled small molecule prostate specific membrane antigen inhibitors with novel polar chelates. *Bioorg Med Chem Lett.* 2013;23:1557-1563.

3. Wilson AA, Jin L, Garcia A, DaSilva JN, Houle S. An admonition when measuring the lipophilicity of radiotracers using counting techniques. *Applied Radiation and Isotopes.* 2001;54:203-208.